日本原子力研究開発機構機関リポジトリ

Japan Atomic Energy Agency Institutional Repository

Title	Study on the evaluation of erosion damage by using laser ultrasonic integrated with a wavelet analysis technique
Author(s)	Wan T., Naoe Takashi, Wakui Takashi, Futakawa Masatoshi, Obayashi Hironari, Sasa Toshinobu
Citation	Journal of Physics; Conference Series, 842(1),p.012010_1-012010_10
Text Version	Published Journal Article
URL	https://jopss.jaea.go.jp/search/servlet/search?5059694
DOI	https://doi.org/10.1088/1742-6596/842/1/012010
Right	

Japan Atomic Energy Agency

You may also be interested in:

Study on the evaluation of erosion damage by using laser ultrasonic integrated with a wavelet analysis technique

T Wan[1,*]**, T Naoe**[1]**, T Wakui**[1]**, M Futakawa**[1]**, H Obayashi**[1] **and T Sasa**[1]

[1] J-PARC Center, Japan Atomic Energy Agency, 2-4 Shirakata, Tokai-mura, Ibaraki 319-1195, Japan

* E-mail: wan.tao@jaea.go.jp

Abstract. Spallation targets are the key components of accelerator driven systems (ADSs) that are being developed in the world. Erosion damages on the target vessels are anticipated. To prevent accidents occurrence due to erosion of spallation target vessel, the damage evaluation technique is desirable. The excited vibration of LBE target vessel will be monitored remotely to establish the technique. In this study, the basic researches were carried out through experiments and numerical simulations to investigate the interaction between ultrasonic waves and damage to understand the correlation between structural vibration and damage degree. Specimens with distributed erosion damage was irradiated by laser shots, and the vibration was detected by a laser vibrometer subsequently. A technique, Wavelet Differential Analysis (WDA), was developed to quantitatively and clearly indicate the differences caused by damage in the vibration signals. The results illustrated that the developed technique is sensitive to erosion damage with small size and is capable of quantitatively evaluating erosion damage. It is expected that the developed techniques can be applied to monitor the real spallation targets in the future.

1. Introduction

The Accelerator Driven Systems (ADSs) are considered to be promising technique approaches to transmute the minor actinides contained in the high-level radioactive wastes effectively and efficiently. Japan Atomic Energy Agency (JAEA) also proposed an ADS adopting Lead-Bismuth Eutectic (LBE) as the spallation material and the coolant [1, 2]. A Beam Window (BW) is a boundary that separates the accelerator and the spallation target. Figure 1 shows the conceptual spallation target BW diagram of LBE-cooled ADS proposed by JAEA. Continuous proton beams with 1.5GeV energy will be injected into LBE through the BW for spallation reaction [3]. Flowing LBE with a speed of 2 m/s will remove the generated heat in LBE and on the BW. Obviously the integrity of BW is critical to the safe operation of ADS because it should withstand severe service conditions. To investigate the following issues for the BW: a) thermal-hydraulic behavior, b) design feasibility & lifetime estimation, and c) effects of beam trips, a LBE spallation target has the same BW structure as the ADS concept will be installed at the ADS Target Test Facility (TEF-T), which will be constructed under the frame work of Japan Proton Accelerator Research Complex (J-PARC) project. The BW will be made of type 316 SS when the operation temperature below 500 °C [4]. To take full advantage of the current J-PARC accelerator, pulsed proton beams (250 kW, 25 Hz, and 0.5 ms pulse duration) will be utilized to bombard the TEF-T LBE spallation target [5, 6].
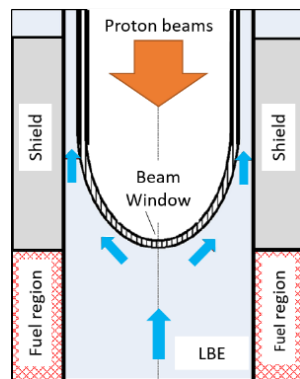
Figure 1. Conceptual diagram of spallation target beam window of LBE-cooled ADS proposed by JAEA.

The design lifetime of future ADS spallation target is several tens of years, while that of the TET-T LBE spallation target is 5000 hours/year on operation. During the operations, several kinds of damages, e.g., fatigue damage, irradiation damage, and erosion damage will be imposed on the BW. Among those sorts of damages, cavitation-induced erosion damage might be a key factor that determines the lifetime of BW. Cavitation might be generated due to negative pressure that attributes to the pressure change in heavy liquid metal (HLM). Several reasons could induce the pressure change, firstly, thermal shocks in HLM due to the pulsed proton beam injections and proton beam trips, and secondly, considerable turbulent flow of HLM. Owing to the high density of HLM, the impact force released on the BW by the collapses of cavitation bubbles close to the BW is very strong and can give rise to the occurrence of cavitation damage on the BW [7, 8]. The lifetime of BW might be significantly shorten by the cavitation damage [9].

Considering the high-radioactive environment around the target, it is expected to develop a remote and noncontact in-situ structural integrity evaluation technique to monitor the service status of target vessel. For this purpose, the laser ultrasonic technique is a reasonable alternative, which adopts a pulsed laser beam remotely and noncontact heating up the objective surface to generate ultrasonic waves and another laser beam to remotely detect the propagation of ultrasonic waves in a certain direction. By employing the laser ultrasonic technique, the dynamic responses of the excited target vessel vibration can be monitored by laser vibrometer or interferometer. It has been reported that the vibration response of target vessel can be affected by the occurrence of cavitation damage for the mercury target in Japan Spallation Neutron Source (JSNS) [10]. On the basis of the detected vibration signals, the structural integrity evaluation technique for the target vessel is expected to be established.

In the present study, the basic researches involving the interactions between ultrasonic waves and cavitation damage were carried out through experiments and numerical simulations in order to investigate correlation between structural vibration and damage degree. In the experiments, laser generation and detection of ultrasonic waves were used to remotely and noncontact evaluate the cavitation damage. A pulsed Nd-YAG laser was employed to impact the specimen, and subsequently the specimen vibration was detected by a Laser Doppler Vibrometer (LDV). In the numerical simulations, a Finite Difference Method (FDM) method was employed to systematically investigate the dependency of vibration signals on damage. Furthermore, a technique, Wavelet Differential Analysis (WDA), was developed to clearly indicate damage dependency in the vibration signals.

In our previous study [11], the vibrational signals obtained from the plate specimens were studied from the viewpoint of propagation behavior of ultrasonic waves and time-of-flight of each wave mode. In this continuous work, new developed method was focused on aims at evaluating the cavitation damage clearly and quantitatively. It is expected the developed technique can be applied to various structures that adopting HLM as spallation/coolant material.

2. Experiments

2.1. Laser ultrasonic system

Figure 2 shows the schematic of the LDV system employed in the experiments. A Q-switched Nd-YAG laser (QUANTEL USA, Ultra 100-55-20) with a wavelength of 532 nm was adopted to impact the specimen without imposing any damage on the surface. The laser beam is 3 mm in diameter with a Gaussian profile. The output energy of the pulsed laser (1 Hz) is 2.5 mJ in 6.5 ns. The bottom surface of the specimen was damaged, which was to simulate the damage on the inner surface of BW, and the damage was detected from the opposite side, i.e., the outside surface of BW.

The vibration of specimen was detected by a LDV (ONOSOKKI, LV-1710) with a He-Ne laser (633 nm, 1 mW), owning a detecting frequency range of 1 Hz–3 MHz. Signals captured by the LDV were stored by using an oscilloscope with a sampling rate of 12.5 MHz. Q-switch signals were used for the triggers of recording LDV signals. Each vibration waveform was averaged by 180 signals to reduce the background noise. A microscope lens focused the He-Ne laser beam to a spot with 3.5 µm in diameter on the specimen surface to obtain a high spatial resolution. The distance between the center point of the Nd-YAG laser beam spot and the He-Ne laser beam spot was fixed to be ca. 5 mm.

2.2. Specimen & Cavitation-induced erosion damage

Figure 3 shows a photograph of the specimen with distributed cavitation damage. The material of specimen is type 316 SS. The damage was imposed on the specimen by using an electro-Magnetic Impact Testing Machine (MIMTM). The detailed characterizations of MIMTM and the distributed cavitation damage was stated in reference [12], and only brief descriptions will be given presently. MIMTM was adopted to simulate the pressure change through the pulsed mechanical impacts of a striker against the HLM. In the MIMTM, mercury is adopted instead of LBE for two main considerations: 1) mercury is in the liquid state at room temperature, whereas the melting point of LBE is ca. 298 K, so that the experiments can be performed more conveniently by using mercury, and 2) some physical properties of mercury, which closely relating to the formation of cavitation bubbles and the released impact force of bubble collapse, are similar to LBE, e.g., density, surface tension. Though the vapor pressure of mercury at room temperature (2.6×10^{-7} MPa) is much higher than that of LBE at the nominal operation temperature (5.8×10^{-13} MPa @ 600 K), both the vapor pressures are far lower than the standard air pressure (0.1 MPa), so the effects of the differences of vapor pressures on cavitation bubble formation can be ignored. The specimen was divided into five areas, and damages with various degrees were conducted at each area, respectively. The maximum peak-to-peak depth of the damage at each area was: (I) 45 µm, (II) 35 µm, (III) 25 µm, (IV) 15 µm, (V) as received. Then the damage at each area was evaluated by the laser ultrasonic systems.
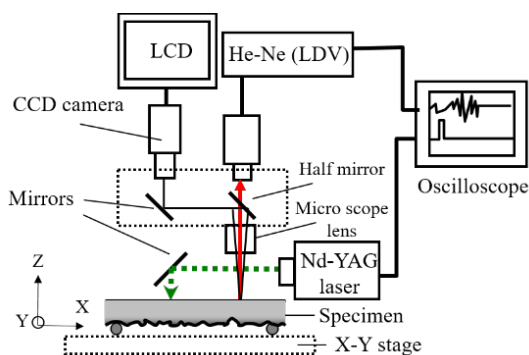

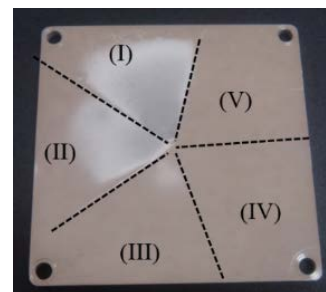**Figure 2.** Schematic drawing of the laser ultrasonic system.

Figure 3. Specimen with distributed cavitation damage: maximum depth of cavitation damage in each area: (I) 45 µm, (II) 35 µm, (III) 25 µm, (IV) 15 µm, (V) as received.

3. Numerical simulations

The numerical simulations were performed using a commercial Finite Difference Method (FDM) code Wave3000 (Cyber Logic). The specific acoustic equation used in Wave3000 is given by [13]:

$$\rho \frac{\partial^2 w}{\partial^2 t} = \left[\mu + \eta \frac{\partial}{\partial t}\right] \nabla^2 w + \left[\lambda + \mu + \phi \frac{\partial}{\partial t} + \frac{\eta}{3}\frac{\partial}{\partial t}\right] \nabla(\nabla \cdot w), \tag{1}$$

where ρ is the material density, kg/m^3; λ is the first Lame constant, N/m^2; μ is the second Lame constant, N/m^2; η is the shear viscosity, N·s/m^2; ϕ is the bulk viscosity, N·s/m^2; ∇ is the gradient operator; $\nabla \cdot$ is the divergence operator; t is the time, s; w is a three-dimensional column vector whose components are the x, y, and z components of the displacement of the medium at location (x, y, z).

To systematically investigate the dependency of ultrasonic wave propagation on number and depth of damage, numerical simulation model with simulated pits was made, as shown in Figure 4(a). The 3D model owns a size of 30×30×2.5 mm^3. The mesh size is 0.1 mm. The maximum Z surface possess an infinite boundary, whereas the other surfaces are "free-free". The source on the upper surface is a pulsed longitudinal sinusoidal wave with a size of 3.2 mm in diameter, a frequency of 1 MHz and a duration of 1 µs. The vibration velocity in the Z-direction was detected by the receiver with 0.2 mm in diameter. Distance of source and receiver is 5.0 mm. Simulated pentahedral pits with various numbers N (ranges from 0 to 900), and depths D (ranges from 0 to 1.4 mm), were established at the bottom of the model. The aspect ratio (depth/width) of simulated pits was 0.5.

It should be mentioned that according to reference [14], wave3000 is a "memory-hungry" program. The approximating required memory is to multiply the number of finite difference grid voxels, say M, by 42. In this study, the maximum depth of the damage is 45 µm. To maintain the structure details of such indent and obtain accurate results, the grid size would be required to be approximately 5 µm. For an object of 30 mm × 30 mm × 2.5 mm, the memory required is about 4400 GB. Obviously, such numerical simulations are impossible to be carried out on a PC. Therefore, to reduce the calculation cost, the depth of damage was selected as 0.4 mm when changing the number of simulated pits, while the number of damage was 900 when varying the depth of simulated pits.

In addition, damages with random profile were also established at the bottom of the model, as shown in Fig. 4(b). The damaged area occupies 90% of the bottom surface, while the maximum depth of random damage was 0.4 and 0.9 mm, respectively.
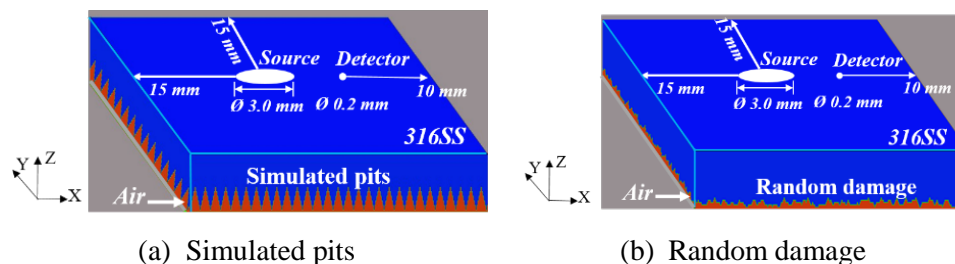

(a) Simulated pits   (b) Random damage

Figure 4. Schematic drawings of numerical simulation models.

4. Wavelet differential analysis

The wavelet differential process [15] for the vibration signals was conducted to clearly indicate the differences between signals. The process is described by Eq. (2) as follows:

$$WDI_D = |Img_D - Img_0|, \tag{2}$$

where WDI is the wavelet differential image, Img is the wavelet image of the vibration signals, and the subscripts D and 0 represents the damage with a depth of D µm and no damage (or D and 0 represents the damage with a number of D and no damage), respectively. Then, the average intensity (I_a) of the wavelet differential image (WDI) was calculated according to equations (3) – (5):

$$I_a = \int^{\Delta f} \int^{\Delta t} V(t, f) \mathrm{d}t \mathrm{d}f, \tag{3}$$

$$\Delta f = f_2 - f_1 \, , \tag{4}$$

$$\Delta t = t_2 - t_1 \, , \tag{5}$$

where the measurement frequency ranges from f_1 to f_2 (Hz), and the measurement time ranges from t_1 to t_2 (s); $V(t, f)$ is the *WDI* intensity (dB) at time t and frequency f, and I_a is the average intensity of the differential image.

5. Results and Discussions

5.1. Time responses of displacement velocity
Figure 5 shows the examples of time responses of the displacement velocity detected from different areas on the specimen with cavitation damage by using the LDV system. The results obtained by locate the detection laser in the opposite side of each damage area. It can be seen from the results that there are two parameters related to the damage. First one is the amplitude of the first positive peak, referred to as V_p (marked in Fig. 5); the second one is the attenuation coefficient (α, marked in Fig. 5) of waveforms, which was defined by the following equation.

$$V_t = V_P e^{-\alpha \cdot t}, \tag{6}$$

where α is the attenuation coefficient, μs^{-1}; V_t is the vibration velocity at time t, m/s, and V_p is the vibration velocity of the first positive peak, m/s.

In the case of the vibrational signal obtained from the damaged specimen, the amplitude of the largest positive peak and the attenuation coefficient of the waveforms increased. As discussed in a previous study, the positive peak was caused by the shear waves that were reflected from the bottom of the specimen, whereas the attenuation was caused by the longitudinal waves that propagate between the upper and bottom surface of the specimen [11].
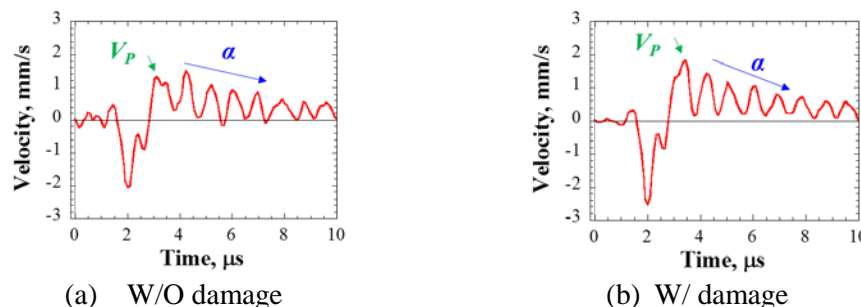

    (a)   W/O damage   (b) W/ damage

Figure 5. Time responses of displacement velocity detected from different areas on the specimen with cavitation damage by using the LDV system.

5.2. Damage evaluation by the amplitude of positive peak
In this subsection, the distributed cavitation damage was evaluated using the LDV system by the positive peak. It is expected to evaluate the maximum depth of damage through the amplitude of positive peak. The numerical simulations were also carried out to evaluate simulated pits and random damage with various depths.

Figure 6 shows the examples of numerical simulation results without damage and with damage. The experimental results shown in Fig. 5 and numerical simulation results shown in Fig. 6 were plotted as functions of the maximum depth of cavitation damage, the results were shown in Fig. 7. From the results it can be seen that the tendency of experimental and the numerical simulation result is coincidence with each other, and the maximum depth of damage can be expressed by the following equation:

$$D = a \times \left(\frac{V_P - V_{P,0}}{V_{P,0}} \right)^b , \tag{7}$$

where D is the maximum depth of damage; V_P is the positive peak of reflected waveforms with damage; $V_{P,0}$ is the positive peak of reflected waveforms without damage; a, b are constants related to the material property.

The cavitation damage reduces the equivalent thickness of the specimen [11], and thus the ultrasonic wave propagation distance from the source to the receiver is affected by the damage. When the damage depth trends to larger, the ultrasonic propagation distance becomes shorter. Therefore, the attenuation of ultrasonic waves due to spreading becomes weaker in the process of propagating from the source to the receiver, so that more energy will be reflected to the receiver and lead to a stronger amplitude of vibration. The variation of positive peak is mainly dominated by the spreading mechanism in the present study.
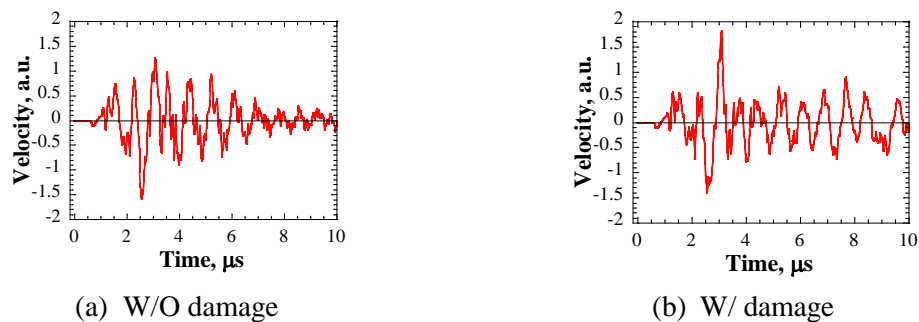

(a) W/O damage   (b) W/ damage

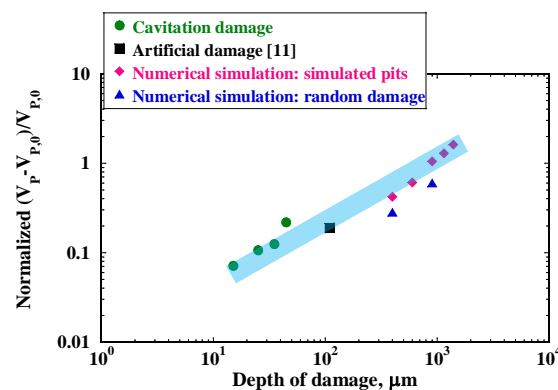**Figure 6.** Time responses of displacement velocity obtained by the numerical simulations.

Figure 7. Damage depth as a function of normalized differential positive peak velocity.

5.3. Damage evaluation by WDA

It can be seen from Fig. 7 that the differences is not very obvious to recognize the damage dependency in cases of the damage depths are considerably small and are close to each other in the experiments. This may because the positive peaks just give the damage information at a time point. It is expected to involve all the information of ultrasonic wave attenuation in both time and frequency domains. The WDA technique provides such an approach. For this purpose, the WDA was used to quantitatively evaluate the damage dependency.

Figure 8 shows the typical examples of *WDI*s for cavitation damages with various maximum depths. Obvious differences can be observed from the *WDI* results. To quantitatively evaluate the differences of *WDI* results, the average intensity of *WDI*s was calculated. Figure 9 shows the average intensity of *WDI*s as a function of damage depth. Clear dependency on damage depth can be recognized from the average intensity results. The results indicates that the average intensity of *WDI*s is very sensitive to damage.

When the maximum depth of the damage increases up to approximately 15 μm, the variation in *WDI* results is mainly indicated in the relatively higher frequency range. If the maximum depth of damage keeps increasing, more obvious differences were shown in the relatively lower frequency range. Cavitation damage develops from isolated micro localized damage to area erosion when the maximum depth increases up to approximately 15μm [16, 17]. At this stage, the number of damage changed obviously while the maximum depth of damage almost keeps a constant. With the further accumulation of cavitation damage, the maximum depth of area erosion keeps increasing. It is assumed that the differences showed in the relatively higher frequency components are mainly attribute to the ultrasonic wave scattering from damage with various numbers, whereas the differences in the relatively lower frequency range is mainly due to the ultrasonic waves scattering from damage with various depths. Detailed discussion will be given in the next sub-section.
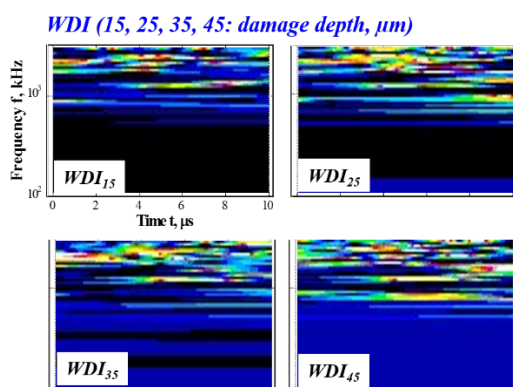

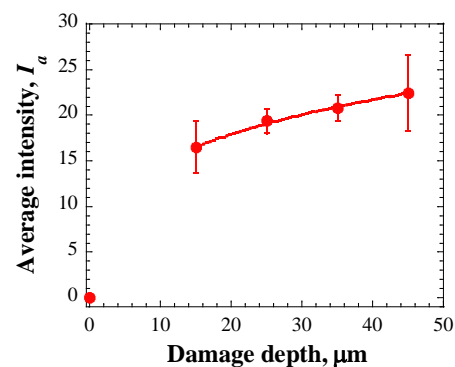**Figure 8.** *WDI* results for the area distributed cavitation damage.

Figure 9. Average intensity of *WDI*s as a function of damage depth.

5.4. Effects of number and depth of damage on WDI results

Numerical simulations were carried out to investigate the effects of number and depth of damage on the *WDI* results. The model with simulated pits was employed for this study. Mesh size of the model was 0.05 mm to provide enough resolution for studying the propagation of ultrasonic waves with relative higher frequencies.

Figure 10 shows the effects of number of damage on the *WDI* results. When the number of damage increases, the differences in the relatively higher frequency region trends more obvious. However, differences can hardly be observed in the relatively lower frequency region. Figure 11 shows the average intensity of *WDI* as a function of each frequency component for various numbers of simulated pits. The damage depth was fixed as 0.4 mm when varying the number of simulated pits. For all the cases, the results can be divided into three regimes: (1) in the region that frequencies are higher than ca. 2 MHz, significantly differences of average intensity appear in the results, which is caused by intense scattering of ultrasonic waves from the damage; (2) when the frequencies locates between ca. 0.8 MHz and 2 MHz, the average intensity shows differences but not so significant as that above ca. 2 MHz. This is considered to be caused by the moderate scattering of ultrasonic waves from the damage; (3) if the frequencies of ultrasonic waves below ca. 0.8 MHz, differences can hardly be observed. Weak scattering of ultrasonic waves from damage occurred in this region.

The phenomenon is related to the relationship between the wavelength of ultrasonic waves and the size of damage. Here, the frequency components of waveforms obtained by simulations are from ca. 0.3 to 19.2 MHz. Assuming that the propagation velocity of ultrasonic waves in stainless steel is 5.7 m/s at room temperature, then the wavelength of the waveforms ranges from ca. 0.30 mm to 19.0 mm. Ultrasonic waves with a frequency of 2 MHz own a wavelength of 2.35 mm, which is ca. 6 times of that of damage depth of 0.4 mm. Ultrasonic waves with such a wavelength or shorter will be strongly scattered by the damage, and the diffusion field distributed in all the scattering directions according to

the Kirchhoff scattering theory [18, 19]. Therefore, if the frequency above 2 MHz, almost all the energy of ultrasonic waves will be diffused due to the strong scattering. It is easy to understand that scattering of ultrasonic waves with frequency above 2 MHz will be enhanced due to the increase of number of damage.

If ultrasonic waves with frequencies locate between ca. 2 MHz and 0.8 MHz encounter the damage, the wavelength of ultrasonic waves is ca. 6 to 16 times of that of damage size. In this case, moderate scattering occurred but the diffusion field in the forward scattering direction is dominant [20], which can be detected by the receiver, and thus *WDI* results show difference in this frequency region but not obvious as the first regime.

If the frequency of ultrasonic wave bellows ca. 0.8 MHz, then the wavelength of the ultrasonic waves keep increasing and trend to far larger than the damage size. As a result, the ultrasonic waves would be weakly scattered by the damage. In this situation, the reflection of ultrasonic waves at the bottom of specimen will obey the Snell's law. Most of the ultrasonic waves will be reflected to the receiver direction. Therefore, the *WDI* results showed tiny differences in this frequency region.

Figure 12 shows the effects of depth of damage on the *WDI* results. The differences were mainly observed in the relatively lower frequency range. Figure 13 shows the average intensity of *WDI* as a function of frequency for various depths of simulated pits. The lower boundary of intense scattering zone shifts from approximately 5.5 MHz to 1 MHz with increasing in the damage depth from 0.2 mm to 1.0 mm. Therefore, *WDI* results display obvious differences in the frequency region between 5.5 MHz and 1 MHz as shown in Fig. 12. On the contrast, ultrasonic waves with frequency higher than 5.5 MHz will not be strongly affected due to the increase of damage depth, because they have already been sufficiently diffused due to the strong scattering when the damage size is 0.2 mm. Therefore, the *WDI* results showed slight differences in the frequency region higher than 5.5 MHz
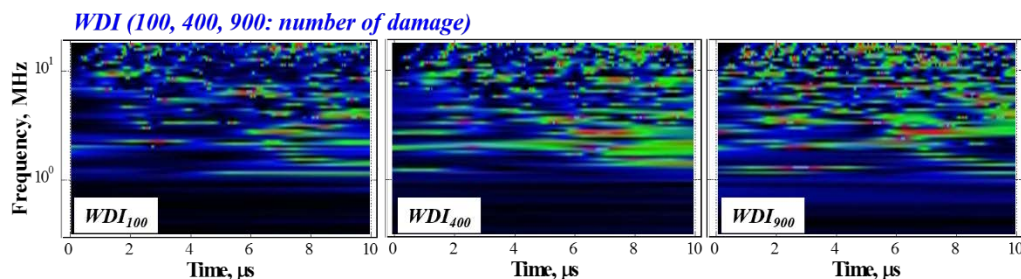

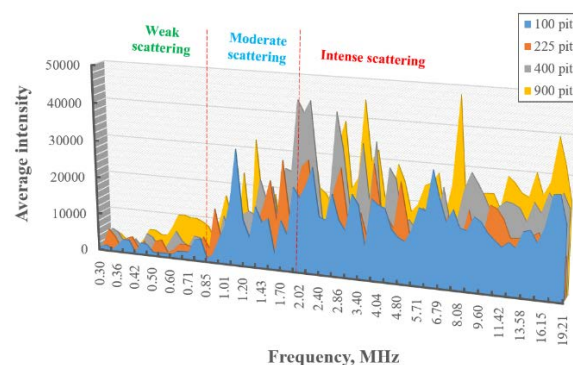**Figure 10.** Effects of number of damage on the *WDI* results.

Figure 11. Average intensity of *WDI* as a function of each frequency component for various numbers of simulated pits.
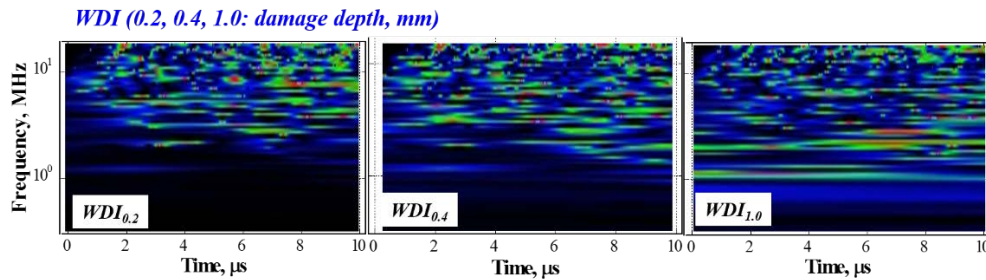
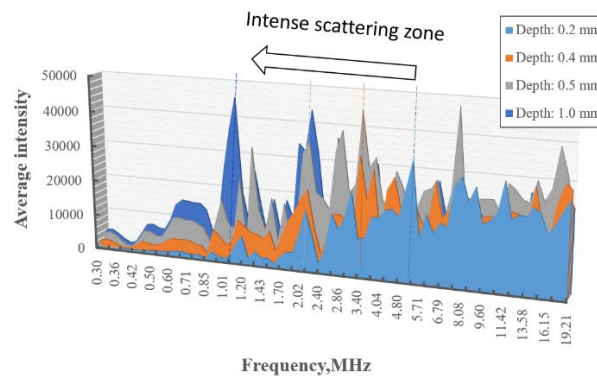**Figure 12.** Effects of depth of damage on the *WDI* results.

Figure 13. Average intensity of *WDI* as a function of each frequency component for various depths of simulated pits.

6. Conclusion

In the present study, the cavitation-induced erosion damage was evaluated by the laser generation and detection of ultrasonic waves. The WDA technique was developed to clearly indicate the damage dependency. The influences of damage number and depth were studied. The results are concluded as the followings:

(1) Damage depth dependency can be quantitatively and clearly indicated by using laser ultrasonic technique integrated with the WDA technique, the developed techniques are very sensitive to the damage with small size.

(2) The variation of number of damage mainly impose effects on scattering of ultrasonic waves with relatively higher frequency, while the variation of depth of damage mainly affects scattering of ultrasonic waves with relative lower frequency.

(3) Scattering of ultrasonic waves from cavitation damage can be divided into three regimes depends on the correlation between ultrasonic wavelength and damage size: 1) ultrasonic waves with wavelength less than 6 times of damage size could be intensely scattered, and the scattering field distributed in all the scattering directions; 2) ultrasonic waves with wavelength approximately 6 to 16 times of damage size could be moderately scattered, and the forward scattering field is dominant; 3) ultrasonic waves with wavelength far larger than damage size could be weakly scattered.

In the future, loop experiments will be carried out, to investigate the dependency of vibration of target vessel filled with liquid on erosion damage, by adopting the techniques presented in this study.

References

[1]   Oigawa H *et al* 2011 *J. Nucl. Mater.* **415** 229
[2]   Tsujimoto K *et al* 2007 *J. Nucl. Sci. Technol.* **44** 483
[3]   Sugawara *et al* 2013 *Ann. Nucl. Energy* **55** 238
[4]   Obayashi H *et al* 2015 *JPS Conf. Proc.* **8** 041002
[5]   Sasa T and Oigawa H 2014 *Plasma and Fusion Research* **9** 4401113
[6]   Sasa T 2015 *Prog. Nucl. Energ.* **82** 64
[7]   Futakawa M, Kogawa H and Hino R 2000 *J. Phys. VI France.* **10** 237
[8]   Futakawa M *et al* 2000 *Nucl. Instrum. Meth. A* **439** 1
[9]   Teshigawara T *et al* 2010 *J. Nucl. Mater.* **398** 23
[10]   Wan T, Naoe T and Futakawa M 2016 J. *Nucl. Mater.* **468** 321
[11]   Wan T *et al* 2014 *Mater. Trans.* **55** 1024
[12]   Wan T *et al* 2013 *Int. J. Mater. Prod. Tec.* **46** 141
[13]   Delsanto P P, Schechter R S and Mignogna R B 1997 *Wave Motion* **26** 329
[14]   CyberLogic Wave3000 manual
[15]   Wan T *et al* 2014 *Appl. Mech. Mater.* **566** 629
[16]   Futakawa M *et al* 2003 *J. Nucl. Sci. Technol.* **40** 895
[17]   Futakawa M *et al* 2005 *J. Nucl. Mater.* **343** 70
[18]   J.A. Ogilvy 1988 *J. Phys. D: Appl. Phys.* **21** 260
[19]   J.A. Ogilvy 1987 *Rep. Prog. Phys.* **50** 1553
[20]   J.A. Ogilvy 1989 *Ultrasonics* **27** 69